Metadata of the article that will be visualized in OnlineFirst

1	Article Title	**Cable-Direct-Driven Robot (CDDR) with Passive SCARA Support: Theory and Simulation**	
2	Journal Name	Journal of Intelligent and Robotic Systems	

3	Corresponding Author	Family Name	**Williams**
4		Particle	
5		Given Name	**Robert L.**
6		Suffix	**II**
7		Organization	Ohio University
8		Division	Department of Mechanical Engineering
9		Address	259 Stocker Center, Athens 45701-2979, OH, USA
10		e-mail	williar4@ohio.edu
11	Author	Family Name	**Trevisani**
12		Particle	
13		Given Name	**Alberto**
14		Suffix	
15		Organization	University of Padova
16		Division	
17		Address	Padova , Italy
18		e-mail	
19	Author	Family Name	**Gallina**
20		Particle	
21		Given Name	**Paolo**
22		Suffix	
23		Organization	University of Trieste
24		Division	
25		Address	Trieste , Italy
26		e-mail	

27	Schedule	Received	6 April 2005
28		Revised	
29		Accepted	2 May 2006

30 Abstract

This article presents a new planar translational cable-direct-driven robot (CDDR) with actuation redundancy and supported against loading normal to the motion plane with a passive planar two-degree-of-freedom SCARA-type (Selective Compliance Assembly Robot Arm) serial manipulator. This allows the robot to resist cable sag without being supported on the motion plane. The proposed robot architecture may assure high payload-to-weight ratio, resistance to forces normal to the plane of motion, and a potentially large workspace. Another benefit is that the passive SCARA has structure to provide end-effector moment resistance, which is not possible with many proposed translational CDDRs. Moreover, the passive robot can also serve as an independent Cartesian metrology system. This article derives the kinematics and dynamics models for the proposed hybrid serial/parallel architecture.

AUTHOR'S PROOF

		Additionally it proposes a dynamic Cartesian controller always ensuring positive cable tensions while minimizing the sum of all the torques exerted by the actuators. Simulation examples are also presented to demonstrate the novel CDDR concept, dynamics, and controller.
31	Keywords separated by ' - '	actuation redundancy - cable-direct-driven robots - dynamic minimum torque estimation - passive support
32	Foot note information	Category (7) – System Modelling/Simulation/Control/Computer–Aided Design/Robot Control/Teleoperation/Moving Robots

J Intell Robot Syst
DOI 10.1007/s10846-006-9043-7

Cable-Direct-Driven Robot (CDDR) with Passive SCARA Support: Theory and Simulation

Alberto Trevisani · Paolo Gallina · Robert L. Williams II

Received: 6 April 2005 / Accepted: 2 May 2006

Abstract This article presents a new planar translational cable-direct-driven robot (CDDR) with actuation redundancy and supported against loading normal to the motion plane with a passive planar two-degree-of-freedom SCARA-type (Selective Compliance Assembly Robot Arm) serial manipulator. This allows the robot to resist cable sag without being supported on the motion plane. The proposed robot architecture may assure high payload-to-weight ratio, resistance to forces normal to the plane of motion, and a potentially large workspace. Another benefit is that the passive SCARA has structure to provide end-effector moment resistance, which is not possible with many proposed translational CDDRs. Moreover, the passive robot can also serve as an independent Cartesian metrology system. This article derives the kinematics and dynamics models for the proposed hybrid serial/parallel architecture. Additionally it proposes a dynamic Cartesian controller always ensuring positive cable tensions while minimizing the sum of all the torques exerted by the actuators. Simulation examples are also presented to demonstrate the novel CDDR concept, dynamics, and controller.

Key words actuation redundancy · cable-direct-driven robots · dynamic minimum torque estimation · passive support

Category (7) – System Modelling/Simulation/Control/Computer–Aided Design/
Robot Control/Teleoperation/Moving Robots

A. Trevisani
University of Padova, Padova, Italy

P. Gallina
University of Trieste, Trieste, Italy

R. L. Williams II (✉)
Department of Mechanical Engineering, Ohio University, 259 Stocker Center, Athens, OH 45701-2979, USA
e-mail: williar4@ohio.edu
URL: http://www.ent.ohiou.edu/~bobw

1. Introduction

Cable-direct-driven robots (CDDRs) are a type of parallel manipulator wherein the end-effector link is supported in-parallel by n cables with n tensioning motors. In addition to the well-known advantages of parallel robots relative to serial robots, CDDRs can have lower mass than other parallel robots. Several CDDRs have been developed to date. An early CDDR is the RoboCrane [2] developed by the National Institute of Standards and Technology (NIST) for use in shipping ports. This device is similar to an upside-down six-degrees-of-freedom (dof) Stewart platform, with six cables instead of hydraulic-cylinder legs. In this system, gravity ensures that cable tension is maintained at all times throughout the system work volume. Another CDDR is Charlotte, developed by McDonnell–Douglas [4] for use on the International Space Station. Charlotte is a rectangular box driven in-parallel by eight cables, with eight tensioning motors mounted on-board (one on each corner). CDDRs can be made lighter, stiffer, safer, and more economical than traditional serial robots since their primary structure consists of lightweight, high load-bearing cables. In addition, a major advantage of CDDRs over existing parallel robots is a larger workspace. On the other hand, one major disadvantage is that cables can only exert tension and cannot push on the end-effector.

Other authors presenting CDDR developments are Aria et al. [1], Mikulas and Yang [7], Shanmugasundram and Moon [10], Yamamoto et al. [14], and Shiang et al. [12].

Roberts et al. [9] present inverse kinematics and fault tolerance of Charlotte-type CDDRs, plus an algorithm to predict if all cables are under tension in a given configuration while supporting the robot weight only. Oh and Agrawal [8] developed a controller to ensure only positive cable tensions for CDDRs. Shen et al. [11] adapt manipulability measures to CDDRs. Choe et al. [5] present stiffness analysis for wire-driven robots. Barette and Gosselin [3] present general velocity and force analysis for planar cable-actuated mechanisms, including dynamic workspace, dependent on end-effector accelerations.

Most CDDRs are designed with actuation redundancy, i.e. more cables than Cartesian motion (or, in contact, wrench-exerting) degrees-of-freedom (except for the RoboCrane, where cable tensioning is provided by gravity) in attempt to avoid configurations where certain wrenches require an impossible pushing force in one or more cables. Despite actuation redundancy, there exist subspaces in the potential workspace where some cables can lose tension. This problem can be exacerbated by CDDR dynamics. A general dynamics controller has been proposed to enable CDDR motions with only positive cable tensions [13].

This article describes the new planar translational CDDR with passive SCARA support, followed by kinematics and dynamics modeling, controller development including a method for attempting to maintain positive cable tensions for all motion, and simulation examples to demonstrate these developments. The features of the proposed CDDR motivating this study include: 1. A high payload-to-weight ratio; 2. A large workspace; 3. Independent Cartesian metrology when adding encoders to the passive SCARA robot; 4. Out-of-plane cable sag can be resisted without supporting end-effector on the plane of motion; 5. The concept can be extended to 3D motion with rotations by adding an active SCARA Z axis and a robot wrist; and 6. The passive SCARA also provides moment resistance at the end-effector, which is not enabled by most proposed CDDRs. For example, consider a drilling tool. If the tool was connected to the end-effector of a translational-only CDDR, vibrations could occur since torsional stiffness would be provided just by cables and end-effector's inertia. Conversely, if the drilling tool was connected to the tip of the second link of the passive SCARA, it would work correctly, since torsional stiffness would be provided by the SCARA structure rather than just by cables. These features combine to make the proposed system a good alternative to existing serial robots, in particular in those industrial applications where large and fast displacements of the end-effector are required while keeping high accuracy throughout the whole workspace (e.g. assembly, fluid dispensing, painting, testing and inspecting). Moreover the hybrid parallel/serial architecture of the system provides superior stiffness even when heavy payloads are handled, compared to existing robot systems.

Of these six CDDR features, the first two are shared by any good cable robot. However, items 3. through 6. are unique to our novel concept and this article.

2. System Description

The hybrid parallel/serial architecture of the Cable-Direct-Driven Robot (CDDR) studied in this work is shown in Figure 1. The manipulator consists of a single end-effector point that can translate in a rectangular planar workspace supported in parallel by four cables controlled by four tensioning actuators. In order to reduce the compliance of the CDDR in the direction normal to the plane of motion, the end-effector is also connected to the free end of a passive planar two-degree-of-freedom serial manipulator (2R SCARA-type) by means of a revolute joint at the end point.

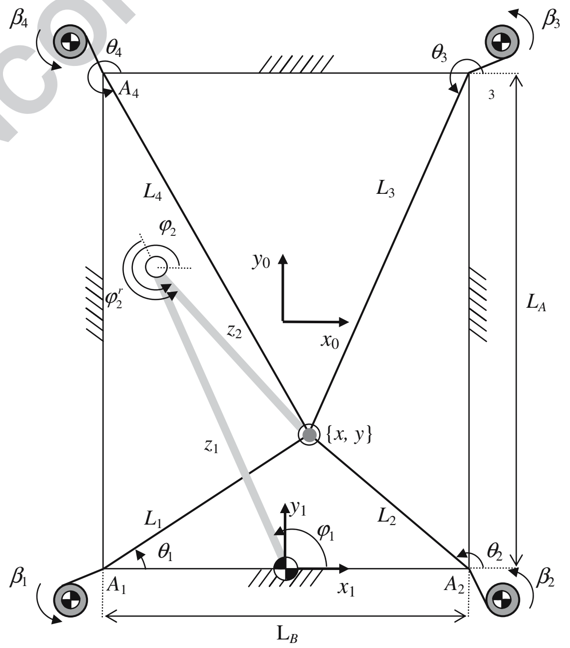

Figure 1 CDDR with passive SCARA support.

In this work it is assumed that only translational degrees of freedom are provided by the four cables. Rotational freedoms could be provided by a serial wrist as proposed in [13]. The studied CDDR has therefore two degrees of actuation redundancy i.e. four cables are used to achieve the two Cartesian degrees-of-freedom $\mathbf{X} = \{x, y\}^T$.

Two reference frames are shown in Figure 1:

- reference frame {0}, whose origin is the centroid of the base polygon,
- reference frame {1}, whose origin is the center of the revolute joint connecting the SCARA serial manipulator to the frame,

The base polygon is a rectangle whose sides have the fixed lengths L_{A} and L_{B}. The ith cable ($i = 1,\ldots, 4$) winds around the ith pulley, whose angle is β_i, and is forced to pass through the fixed vertex A_i of the base polygon. The length of the ith cable, measured from the vertex A_i to the end-effector point $\{x, y\}$, is denoted as L_i, and the cable angle is θ_i. Finally, z_1 and z_2 are the lengths of the two links of the serial manipulator, and φ_1 and φ_2 are the absolute angles between the frame and the links. The symbol φ_2^r instead denotes the relative angle between link 1 and link 2. The serial manipulator is supposed to be attached to the frame at the midpoint of one side of the base polygon. It can be easily proved that such a choice minimizes the overall length of the support links.

3. Kinematics Modeling

This section presents the forward and inverse kinematics analysis for the studied planar CDDR. Kinematics analysis is concerned with relating the active joint variables and rates (i.e. $\boldsymbol{\beta}$, $\dot{\boldsymbol{\beta}}$ and $\ddot{\boldsymbol{\beta}}$, where $\boldsymbol{\beta} \in \mathbb{R}^4$ is the vector of the pulley angles: $\boldsymbol{\beta} = \{\beta_1, \beta_2, \beta_3, \beta_4\}^T$) to the Cartesian position and rate variables of the end-effector point (i.e. $\mathbf{X}$, $\dot{\mathbf{X}}$ and $\ddot{\mathbf{X}}$, with $\mathbf{X} \in \mathbb{R}^2$) and the serial manipulator joint variables and rates (i.e. $\boldsymbol{\varphi}$, $\dot{\boldsymbol{\varphi}}$, and $\ddot{\boldsymbol{\varphi}}$ where $\varphi \in \mathbb{R}^2$ is the vector of the joint angles: $\boldsymbol{\varphi} = \{\varphi_1\ \varphi_2\}^T$).

Since the joints of the passive serial manipulator are not actuated directly, their values and rates can be always determined indirectly through the Cartesian position and rate variables of the end-effector point. It is therefore appropriate to keep the computation of the $\boldsymbol{\varphi}$, $\dot{\boldsymbol{\varphi}}$, and $\ddot{\boldsymbol{\varphi}}$ separate from the computation of the relations among the joint variables $\boldsymbol{\beta}$, $\dot{\boldsymbol{\beta}}$ and $\ddot{\boldsymbol{\beta}}$, and the Cartesian variables $\mathbf{X}$, $\dot{\mathbf{X}}$ and $\ddot{\mathbf{X}}$. If all the cables always remain in tension, the studied CDDR kinematics is similar to in-parallel-actuated robot kinematics, combined with serial robot kinematics. However, with CDDRs the joint space is overconstrained with respect to the Cartesian space due to the redundant actuation.

3.1. Position Kinematics

The objective of the forward position kinematics problem is determining the Cartesian position $\mathbf{X}$ of the end-effector given the pulley angles $\boldsymbol{\beta}$. This problem is overconstrained. Once $\mathbf{X}$ is determined, in order to complete the analysis it is also necessary to determine the joint angles $\boldsymbol{\varphi}$ via the serial robot inverse pose kinematics. Let $L_0 = \sqrt{\left({}^{L_{\mathrm{A}}}\!/_2\right)^2 + \left({}^{L_{\mathrm{B}}}\!/_2\right)^2}$ be the length of each cable when the end-effector is at the origin of the reference frame {0} (i.e. $\{x, y\}0 = \{0, 0\}_0$). Also assume that all angles β_i are set to zero at this point. At any position, the length L_i of the ith cable can be computed from the measured pulley angles through the following equation:

$$L_i = L_0 - r_i \beta_i \tag{1}$$

where r_i is the radius of the ith pulley. In this work it is assumed that all the pulley radii are identical: $r_i = r$. Because the forward position problem is overconstrained, once the length of two cables is known, it is possible to compute the two Cartesian coordinates $\{x, y\}0$. Any two cables could be used to obtain the solution. Henceforth, the cables 1 and 2 will be used. The solution to the problem can be computed by the intersection of two circles, one centered at A_1, with radius L_1, and the second centered at A_2 with radius L_2. The result, expressed in frame $\{0\}$, is:

$$\mathbf{X} = \left\{ \begin{array}{c} \dfrac{L_{\mathrm{B}}^2 + L_1^2 - L_2^2 - L_{\mathrm{B}}}{2L_{\mathrm{B}}} \\ \sqrt{L_1^2 - \left(\dfrac{L_{\mathrm{B}}^2 + L_1^2 - L_2^2}{2L_{\mathrm{B}}}\right)^2} - \dfrac{L_{\mathrm{A}}}{2} \end{array} \right\}_0 \tag{2}$$

By combining (1) and (2) it is possible to get an explicit expression for the Cartesian position $\mathbf{X} = \mathbf{X}(\boldsymbol{\beta})$. In particular, when considering cables 1 and 2, $\mathbf{X}(\boldsymbol{\beta})$ takes the form:

$$\mathbf{X} = \left\{ \begin{array}{c} \dfrac{r^2\left(\beta_1^2 - \beta_2^2\right)}{2L_{\mathrm{B}}} + \dfrac{rL_0(\beta_2 - \beta_1)}{L_{\mathrm{B}}} \\ \sqrt{(L_0 - \beta_1 r)^2 - \left(\dfrac{L_{\mathrm{B}}}{2} + \dfrac{r^2\left(\beta_1^2 - \beta_2^2\right)}{2L_{\mathrm{B}}} + \dfrac{rL_0(\beta_2 - \beta_1)}{L_{\mathrm{B}}}\right)^2} - \dfrac{L_{\mathrm{A}}}{2} \end{array} \right\}_0 \tag{3}$$

When the position $\mathbf{X}$ of the end-effector is known in the reference frame $\{0\}$, the position of the CDDR links (i.e. the joint coordinates $\boldsymbol{\varphi} = \{\varphi_1 \; \varphi_2\}^T$) can be determined by solving the inverse kinematics problem for the serial manipulator. It is well known that there exists an analytical solution to this problem, with two solution branches (see e.g. [6]). If we first compute the end-effector position in the reference frame $\{1\}$ by the relation $\{\mathbf{X}\}_1 = \{x_1 \; y_1\}^T = \{\mathbf{X}\}_0 + \{0 \; L_A/2\}^T$, then it is possible to determine the angle φ_2^r through the relation:

$$\cos\varphi_2^r = \frac{x_1^2 + y_1^2 - z_2^2 - z_1^2}{2z_1 z_2} \Rightarrow \varphi_2^r \mathrm{a}\tan_2\left(\pm\sqrt{1 - \cos^2\varphi_2^r}, \cos\varphi_2^r\right).$$

The result is:

$$\boldsymbol{\varphi} = \left\{ \begin{array}{c} \varphi_1 \\ \varphi_2 \end{array} \right\} = \left\{ \begin{array}{c} \mathrm{a}\tan_2(y_1, x_1) - \mathrm{a}\tan_2\left(z_2 \sin\varphi_2^r, z_2\cos\varphi_2^r + z_1\right) \\ \varphi_2^r + \varphi_1 \end{array} \right\}.$$

Conversely, the end-effector coordinates in the reference frame $\{0\}$ are related to the joint coordinates by the simple forward position relationship:

$$\mathbf{X} = \left\{ \begin{array}{c} z_1 \cos\varphi_1 + z_2 \cos\varphi_2 \\ -\dfrac{L_{\mathrm{A}}}{2} + z_1 \sin\varphi_1 + z_2 \sin\varphi_2 \end{array} \right\}_0 \tag{4}$$

Hereafter it will be assumed that all the Cartesian coordinates are expressed in the reference frame $\{0\}$ and the subscript '0' will hence be omitted. The objective of the inverse position kinematics problem is determining the pulley angles β given the Cartesian position $\mathbf{X}$ of the end-effector. This problem has a simple geometrical solution: The length L_i of the ith cable can be computed as:

$$L_i = \sqrt{(x - A_{ix})^2 + (y - A_{iy})^2} \tag{5}$$

where A_{ix} and A_{iy} are the coordinates of the ith vertex in $\{0\}$. The expression of β can be obtained by substituting (5) into (1) for each pulley:

$$\boldsymbol{\beta} = \begin{Bmatrix} \beta_1 \\ \beta_2 \\ \beta_3 \\ \beta_4 \end{Bmatrix} = \frac{1}{r} \begin{Bmatrix} L_0 - \sqrt{(x - A_{1x})^2 + (y - A_{1y})^2} \\ L_0 - \sqrt{(x - A_{2x})^2 + (y - A_{2y})^2} \\ L_0 - \sqrt{(x - A_{3x})^2 + (y - A_{3y})^2} \\ L_0 - \sqrt{(x - A_{4x})^2 + (y - A_{4y})^2} \end{Bmatrix} \tag{6}$$

3.2. Velocity Kinematics

The time derivative of (6) provides the solution to the inverse velocity kinematics problem for the CDDR:

$$\dot{\boldsymbol{\beta}} = \frac{\partial \dot{\boldsymbol{\beta}}}{\partial \mathbf{X}} \dot{\mathbf{X}} = -\frac{1}{r} \begin{bmatrix} \frac{x - A_{1x}}{L_1} & \frac{y - A_{1y}}{L_1} \\ \frac{x - A_{2x}}{L_2} & \frac{y - A_{2y}}{L_2} \\ \frac{x - A_{3x}}{L_3} & \frac{y - A_{3y}}{L_3} \\ \frac{x - A_{4x}}{L_4} & \frac{y - A_{4y}}{L_4} \end{bmatrix} \begin{Bmatrix} \dot{x} \\ \dot{y} \end{Bmatrix} \tag{7}$$

Unlike the inverse velocity (7), the forward velocity solution is subject to singularities. The singularity conditions are derived from the determinants of the three possible 2×2 square submatrices of the Jacobian matrix $\frac{\partial \boldsymbol{\beta}}{\partial \mathbf{X}}$. Practically, as proved by Williams and Gallina [13], the singularities occur when two cables lie along a straight line, at the edges of the theoretical kinematic workspace. Below, the solution $\dot{\mathbf{X}}$ of the forward velocity problem is computed from the angular velocities of two arbitrarily chosen pulleys. As in the previous section, cables 1 and 2 are used. Instead of inverting the submatrix composed by the first two rows of $\frac{\partial \dot{\boldsymbol{\beta}}}{\partial \mathbf{X}}$, we get the solution by directly differentiating (3) with respect to time:

$$\dot{\mathbf{X}} = \begin{Bmatrix} \dot{x} \\ \dot{y} \end{Bmatrix} = \frac{\partial \mathbf{X}}{\partial \boldsymbol{\beta}_{12}} \dot{\boldsymbol{\beta}}_{12} = \begin{bmatrix} \frac{\partial x}{\partial \beta_1} & \frac{\partial x}{\partial \beta_2} \\ \frac{\partial y}{\partial \beta_1} & \frac{\partial y}{\partial \beta_2} \end{bmatrix} \begin{Bmatrix} \dot{\beta}_1 \\ \dot{\beta}_2 \end{Bmatrix} \tag{8}$$

where $\dot{\boldsymbol{\beta}}_{12} \in \mathbb{R}^2$ is the vector $\left\{\dot{\beta}_1, \dot{\beta}_2\right\}^T$ containing the first two pulley rates and:

$$\frac{\partial x}{\partial \beta_1} = \frac{r^2 \beta_1}{L_{\mathrm{B}}} - \frac{r L_0}{L_{\mathrm{B}}}; \ \frac{\partial x}{\partial \beta_2} = -\frac{r^2 \beta_2}{L_{\mathrm{B}}} + \frac{r L_0}{L_{\mathrm{B}}}$$

$$\frac{\partial y}{\partial \beta_1} = \frac{1}{y + \frac{L_{\mathrm{A}}}{2}} \left[-r L_0 + r^2 \beta_1 - \frac{\partial x}{\partial \beta_1} \left(x + \frac{L_{\mathrm{B}}}{2} \right) \right]; \ \frac{\partial y}{\partial \beta_2} = -\frac{1}{y + \frac{L_{\mathrm{A}}}{2}} \left(x + \frac{L_{\mathrm{B}}}{2} \right) \frac{\partial x}{\partial \beta_2}$$

These equations show that when the end effector lies on $\overline{A_1 A_2}$ (i.e. when $y = -\frac{L_A}{2}$), both $\frac{\partial y}{\partial \beta_1}$ and $\frac{\partial y}{\partial \beta_2}$ become infinite and the CDDR is in a singular configuration. In order to complete the solution of the velocity kinematics problem, we also require the serial manipulator joint angle rates. By differentiating (4) with respect to time, the result is:

$$\dot{\mathbf{X}} = \begin{Bmatrix} \dot{x} \\ \dot{y} \end{Bmatrix} = \begin{bmatrix} -z_1 \sin\varphi_1 & -z_2 \sin\varphi_2 \\ z_1 \cos\varphi_1 & z_2 \cos\varphi_2 \end{bmatrix} \begin{Bmatrix} \dot{\varphi}_1 \\ \dot{\varphi}_2 \end{Bmatrix} := \mathbf{J_k}\dot{\boldsymbol{\varphi}} \tag{9}$$

The computation of $\dot{\boldsymbol{\varphi}}$ is possible only if the determinant of the Jacobian matrix $\mathbf{J_k}$ is not zero (i.e. if $\varphi_2 \neq \varphi_1$, $\varphi_2 \neq \varphi_1 + \pi$). If the Jacobian matrix $\mathbf{J_k}$ is non-singular, the serial inverse velocity solution is:

$$\dot{\boldsymbol{\varphi}} = \mathbf{J_k}^{-1}\dot{\mathbf{X}} \tag{10}$$

Hence the presence of the passive serial manipulator introduces further singular configurations to the CDDR. These singularities can be prevented within the manipulator workspace by appropriate choice of the link lengths.

3.3. Acceleration Kinematics

The solution to the CDDR forward acceleration kinematics problem can be obtained by differentiating (8) with respect to time. The following equation results:

$$\ddot{\mathbf{X}} = \frac{\partial \mathbf{X}}{\partial \boldsymbol{\beta}_{12}}\ddot{\boldsymbol{\beta}}_{12} + \frac{\mathrm{d}}{\mathrm{d}t}\left(\frac{\partial \mathbf{X}}{\partial \boldsymbol{\beta}_{12}}\right)\dot{\boldsymbol{\beta}}_{12} = \frac{\partial \mathbf{X}}{\partial \boldsymbol{\beta}_{12}}\ddot{\boldsymbol{\beta}}_{12} + \mathbf{C_a}\dot{\boldsymbol{\beta}}_{12}^2 + \mathbf{C_b}\dot{\beta}_1\dot{\beta}_2 \tag{11}$$

where:

$$\mathbf{C_a} = \begin{bmatrix} \dfrac{\partial^2 x}{\partial \beta_1^2} & \dfrac{\partial^2 x}{\partial \beta_2^2} \\ \dfrac{\partial^2 y}{\partial \beta_1^2} & \dfrac{\partial^2 y}{\partial \beta_2^2} \end{bmatrix}; \dot{\boldsymbol{\beta}}_{12}^2 = \begin{Bmatrix} \dot{\beta}_1^2 \\ \dot{\beta}_2^2 \end{Bmatrix};$$

$$\mathbf{C_b} = \begin{Bmatrix} 2\dfrac{\partial^2 x}{\partial \beta_1 \partial \beta_2} \\ 2\dfrac{\partial^2 y}{\partial \beta_1 \partial \beta_2} \end{Bmatrix} = \begin{Bmatrix} 0 \\ 2\dfrac{\partial x}{\partial \beta_2}\left[\dfrac{\partial y}{\partial \beta_1}\left(x + \dfrac{L_B}{2}\right) - \dfrac{\partial x}{\partial \beta_1}\left(y + \dfrac{L_A}{2}\right)\right] \Big/ \left(y + \dfrac{L_A}{2}\right)^2 \end{Bmatrix}$$

The elements of matrix $\mathbf{C_a}$ can be computed as follows:

$$\frac{\partial^2 x}{\partial \beta_1^2} = \frac{r^2}{L_B}; \frac{\partial^2 x}{\partial \beta_2^2} = -\frac{r^2}{L_B}$$

$$\frac{\partial^2 y}{\partial \beta_1^2}=\left\{\left[r^2-\left(\frac{\partial x}{\partial \beta_2}\right)^2-\left(x+\frac{L_{\mathrm{B}}}{2}\right)\frac{r^2}{L_{\mathrm{B}}}\right]\left(y+\frac{L_{\mathrm{A}}}{2}\right)\right.$$
$$\left.-\left[rL_0+r^2\beta_1-\frac{\partial x}{\partial \beta_1}-\left(x+\frac{L_{\mathrm{B}}}{2}\right)\right]\left(\frac{\partial y}{\partial \beta_1}\right)\right\}\Big/\left(y-\frac{L_{\mathrm{A}}}{2}\right)^2$$

$$\frac{\partial^2 y}{\partial \beta_1^2}=-\left\{\left[\left(\frac{\partial x}{\partial \beta_2}\right)^2+\left(x+\frac{L_{\mathrm{B}}}{2}\right)\left(-\frac{r^2}{L_{\mathrm{B}}}\right)\right]\left(y+\frac{L_{\mathrm{A}}}{2}\right)\right.$$
$$\left.-\frac{\partial x}{\partial \beta_2}\frac{\partial y}{\partial \beta_2}\left(x+\frac{L_{\mathrm{B}}}{2}\right)\right\}\Big/\left(y+\frac{L_{\mathrm{A}}}{2}\right)^2$$

Finally, the solution to the CDDR inverse acceleration kinematics problem is:

$$\ddot{\boldsymbol{\beta}}=\frac{\mathrm{d}}{\mathrm{d}t}\left(\frac{\partial \boldsymbol{\beta}}{\partial \mathbf{X}}\right)\dot{\mathbf{X}}+\frac{\partial \boldsymbol{\beta}}{\partial \mathbf{X}}\ddot{\mathbf{X}}$$

$$=-\frac{1}{r}\begin{bmatrix}\frac{x-A_{1x}}{L_1} & \frac{y-A_{1y}}{L_1}\\ \frac{x-A_{2x}}{L_2} & \frac{y-A_{2y}}{L_2}\\ \frac{x-A_{3x}}{L_3} & \frac{y-A_{3y}}{L_3}\\ \frac{x-A_{4x}}{L_4} & \frac{y-A_{4y}}{L_4}\end{bmatrix}\begin{Bmatrix}\ddot{x}\\ \ddot{y}\end{Bmatrix}-\frac{1}{r}\begin{bmatrix}\frac{L_1^2-(x-A_{1x})^2}{L_1^3} & \frac{L_1^2-(y-A_{1y})^2}{L_1^3}\\ \frac{L_2^2-(x-A_{2x})^2}{L_2^3} & \frac{L_2^2-(y-A_{2y})^2}{L_2^3}\\ \frac{L_3^2-(x-A_{3x})^2}{L_3^3} & \frac{L_3^3-(y-A_{3y})^2}{L_3^3}\\ \frac{L_4^2-(x-A_{4x})^2}{L_4^3} & \frac{L_4^2-(y-A_{4y})^2}{L_4^3}\end{bmatrix}$$

$$\begin{Bmatrix}\dot{x}^2\\ \dot{y}^2\end{Bmatrix}-\frac{2}{r}\begin{bmatrix}\frac{(x-A_{1x})(y-A_{1y})}{L_1^3}\\ \frac{(x-A_{2x})(y-A_{2y})}{L_2^3}\\ \frac{(x-A_{3x})(y-A_{3y})}{L_3^3}\\ \frac{(x-A_{3x})(y-A_{4y})}{L_4^3}\end{bmatrix}\dot{x}\dot{y} \tag{12}$$

and for the serial manipulator:

$$\begin{Bmatrix}\ddot{\varphi}_1\\ \ddot{\varphi}_2\end{Bmatrix}=\begin{bmatrix}-z_1\sin\varphi_1 & -z_2\sin\varphi_2\\ z_1\cos\varphi_1 & z_2\cos\varphi_2\end{bmatrix}^{-1}$$
$$\left\{\begin{Bmatrix}\ddot{x}_1\\ \ddot{y}_2\end{Bmatrix}-\begin{bmatrix}-z_1\cos\varphi_1 & -z_2\cos\varphi_2\\ z_1\sin\varphi_1 & -z_2\sin\varphi_2\end{bmatrix}\begin{Bmatrix}\dot{\varphi}_1^2\\ \dot{\varphi}_2^2\end{Bmatrix}\right\}:=\mathbf{J}_{\mathbf{k}}^{-1}\ddot{\mathbf{X}}-\mathbf{W}\left\{\mathbf{J}_{\mathbf{k}}^{-1}\dot{\mathbf{X}}\right\}^2 \tag{13}$$

where the matrix $\mathbf{J_k}$ is defined in (9) and

$$\mathbf{W}=\begin{bmatrix}-z_1\sin\varphi_1 & -z_2\sin\varphi_2\\ z_1\cos\varphi_1 & z_2\cos\varphi_2\end{bmatrix}^{-\mathbf{1}}\begin{bmatrix}-z_1\cos\varphi_1 & -z_2\cos\varphi_2\\ -z_1\sin\varphi_1 & -z_2\sin\varphi_2\end{bmatrix}.$$

4. Dynamics Modeling

This section presents dynamics modeling for the studied planar CDDR with passive SCARA support. Dynamics modeling is concerned with relating the Cartesian translational motion of the moving CDDR point to the required active joint torques. In the dynamics model derived in this section Coulomb friction is ignored and it is assumed that the links are rigid and the cables are massless and perfectly stiff (i.e. the cables inertias and spring stiffnesses are neglected). Gravity is also ignored because it is assumed to be perpendicular to the CDDR plane. Despite these simplifications, the resulting model is coupled and nonlinear. The overall system dynamics model is obtained by combining the equations of motion of the three CDDR sub-systems: The end-effector, the actuators, and the serial manipulator.

4.1. End-Effector Dynamics Model

Figure 2 shows the free-body diagram (FBD) for the end effector. Let m be the mass of the end-effector, $\mathbf{F_T} = \{F_{Tx}\ F_{Ty}\}^{\mathrm{T}}$ be the resultant of all four cable tensions t_i, and $\mathbf{F_S} = \{F_{Sx}\ F_{Sy}\}^{\mathrm{T}}$ be the force exerted on the end effector by the serial manipulator. The dynamics model for the end-effector is given by:

$$\mathbf{F_T} + \mathbf{F_S} = \mathbf{m}\ddot{\mathbf{X}} \tag{14}$$

where $\mathbf{m} = \begin{pmatrix} m & 0 \\ 0 & m \end{pmatrix}$ is the Cartesian mass matrix of the end-effector. The force $\mathbf{F_T}$ exerted by the cables on the end-effector can be computed through the following expression:

$$\mathbf{F_T} = \left\{F_{Tx}\ F_{Ty}\right\}^{\mathrm{T}} = \begin{bmatrix} -\cos\theta_1 & -\cos\theta_2 & -\cos\theta_3 & -\cos\theta_4 \\ -\sin\theta_1 & -\sin\theta_2 & -\sin\theta_3 & -\sin\theta_4 \end{bmatrix} \{t_1\ t_2\ t_3\ t_4\}^T := \mathbf{ST} \tag{15}$$

where $\mathbf{T} \in \mathbb{R}^4$ is the vector of cable tensions, and $\mathbf{S}$ is the 2×4 pseudostatics Jacobian matrix whose elements are trigonometric functions of the cable angles, which are calculated as:

$$\theta_i = \mathrm{a}\tan_2\left(\frac{y - A_{iy}}{x - A_{ix}}\right). \tag{16}$$

Figure 2 End-effector point mass FBD.

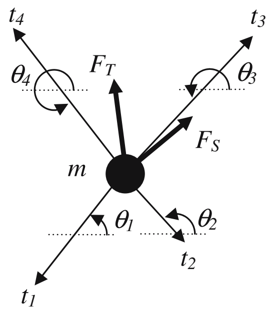

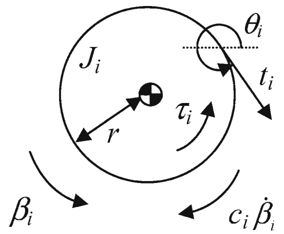

Figure 3 ith Actuator/Pulley FBD.

4.2. Actuator Dynamics Model

The CDDR end-effector is driven by four cables winding around four independent pulleys. Each pulley is actuated by a motor exerting torque τ_i. A lumped rotational inertia J_i is introduced in the model for each motor shaft/pulley system. A linear model for friction is also provided in the model through viscous damping coefficients c_i. The free-body diagram of the ith actuator is shown in Figure 3. The actuators' dynamics equations are expressed by the matrix relationship:

$$\boldsymbol{\tau} - \mathbf{J}\ddot{\boldsymbol{\beta}} - \mathbf{C}\dot{\boldsymbol{\beta}} = r\mathbf{T} \tag{17}$$

where $\mathbf{J} = \begin{bmatrix} J_1 & & 0 \\ & \ddots & \\ 0 & & J_4 \end{bmatrix}$ and $\mathbf{C} = \begin{bmatrix} c_1 & & 0 \\ & \ddots & \\ 0 & & c_4 \end{bmatrix}$ are diagonal matrices with the actuators' rotational inertias and rotational viscous damping coefficients on the diagonal. (17) only holds true when torque on each motor is large enough to make all cables remain in tension at all times.

4.3. Serial Manipulator Dynamics Model

Under the positive tension assumption just made, by combining (14), (15), and (17), the following equation can be obtained for the CDDR dynamics:

$$\mathbf{S}\boldsymbol{\tau} = r\mathbf{m}\ddot{\mathbf{X}} + \mathbf{SJ}\ddot{\boldsymbol{\beta}} + \mathbf{SC}\dot{\boldsymbol{\beta}} - r\mathbf{F}_{\mathrm{S}} \tag{18}$$

The force $\mathbf{F}_{\mathrm{S}}$ exerted by the serial manipulator on the end-effector can be computed by direct application of the Newton–Euler's laws to the two links comprising the serial manipulator [6]. The free body diagrams for the two links are shown in Figure 4. For simplicity, in Figure 4 the links are drawn as straight rods, and the link centers of mass are placed at the midpoints of the links (i.e. uniform mass density is assumed). However, the equilibrium equations adopted hold for any link shape and mass distribution. Moreover, it is important to recall that the joints of the passive supporting SCARA manipulator are not directly actuated. As a consequence the joint inertias, as well as Coulomb and viscous friction, are likely to be negligible, and therefore are not accounted for in the model.

The dynamics equations for link 1 and 2 are, respectively:

$$\begin{cases} X_1^r + X_2^r + F_{\mathrm{in}1x} = 0 \\ Y_1^r + Y_2^r + F_{\mathrm{in}1y} = 0 \\ C_{\mathrm{in}1}^0 - z_1 X_2^r \sin\varphi_1 + z_1 Y_2^r \cos\varphi_1 = 0 \end{cases} \tag{19}$$

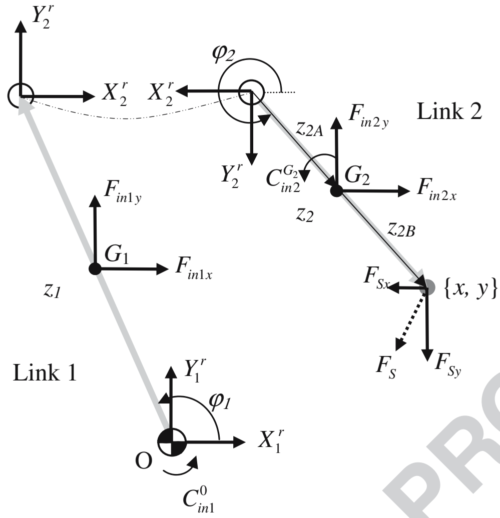

Figure 4 Serial robot link FBDs.

$$\begin{cases} -X_2^r + F_{\text{in}2x} - F_{\text{S}x} = 0 \\ -Y_2^r + F_{\text{in}2y} - F_{\text{S}y} = 0 \\ C_{\text{in}2}^{G_2} - z_{2A} X_2^r \sin\varphi_2 + z_{2A} Y_2^r \cos\varphi_2 + z_{2B} F_{\text{S}x} \sin\varphi_2 - z_{2B} F_{\text{S}y} \cos\varphi_2 = 0 \end{cases} \quad (20)$$

where the subscript *in* denotes the inertial terms: For example, $F_{\text{in}1x}$ is the opposite of the product of the mass of link 1 and the component along the axis x_0 (see Figure 1) of the acceleration of the center of mass G_1, while $C_{\text{in}2}^{G_2}$ is the opposite of the product of the moment of inertia of link 2 about G_2 ($I_2^{G_2}$) and the angular acceleration of the link. By combining (19) and (20), it is possible to eliminate the reaction forces X_j^r and Y_j^r ($j = 1, 2$) and to obtain $\mathbf{F_S}$. The following expression holds in matrix form:

$$\mathbf{F_S} = \mathbf{M_S}\ddot{\mathbf{X}}_{\mathbf{G}_2} + \mathbf{I_{NS}}\ddot{\boldsymbol{\varphi}} \quad (21)$$

where $\mathbf{M_S}$ and $\mathbf{I_{NS}}$ are the matrices collecting the terms which multiply the translational acceleration $\ddot{\mathbf{X}}_{\mathbf{G}_2} = \left\{\ddot{x}_{G_2}\ \ddot{y}_{G_2}\right\}^T$ of the center of mass of link 2 and the angular accelerations of the two links $\ddot{\boldsymbol{\varphi}} = \{\ddot{\varphi}_1\ \ddot{\varphi}_2\}^T$:

$$\mathbf{M_S} = \frac{1}{z_1\left(z_{2A} + z_{2B}\right)\sin\left(\varphi_1 - \varphi_2\right)} \begin{bmatrix} m_2 z_1 \sin\varphi_2\left[-\left(z_{2A} + z_{2B}\right)\cos\varphi_2 + z_{2A}\cos\varphi_1\right] & m_2 z_1 z_{2B}\cos\varphi_1\cos\varphi_2 \\ -m_2 z_1 z_{2B}\sin\varphi_1\sin\varphi_2 & -m_2 z_1\left[\left(z_{2A} + z_{2B}\right)\cos\varphi_1\sin\varphi_2 + z_{2A}\sin\varphi_1\cos\varphi_2\right] \end{bmatrix}$$

$$\mathbf{I_{NS}} = \frac{1}{z_1\left(z_{2A} + z_{2B}\right)\sin\left(\varphi_1 - \varphi_2\right)} \begin{bmatrix} I_1^0\left(z_{2A} + z_{2B}\right)\cos\varphi_2 & -I_2^{G_2} z_1\cos\varphi_1 \\ I_1^0\left(z_{2A} + z_{2B}\right)\sin\varphi_2 & -I_2^{G_2} z_1\sin\varphi_1 \end{bmatrix}$$

A more useful expression for $\mathbf{F_S}$ can be obtained by making explicit the dependence of $\ddot{\mathbf{X}}_{G_2}$ and $\ddot{\boldsymbol{\varphi}}$ on the Cartesian position velocity and acceleration of the end-effector. In (13) the dependence has already been established for $\ddot{\boldsymbol{\varphi}}$; $\ddot{\mathbf{X}}_{G_2}$ can instead been computed as follows:

$$\ddot{\mathbf{X}}_{G_2} = \begin{Bmatrix} \ddot{x}_{G_2} \\ \dot{y} \end{Bmatrix} = \begin{bmatrix} -z_1 \sin\varphi_1 & -z_{2A}\sin\varphi_2 \\ z_1 \cos\varphi_1 & z_{2A}\cos\varphi_2 \end{bmatrix} \begin{Bmatrix} \dot{\beta}_1 \\ \dot{\beta}_2 \end{Bmatrix}$$

$$\begin{Bmatrix} \ddot{\varphi}_1 \\ \ddot{\varphi}_2 \end{Bmatrix} + \begin{bmatrix} -z_1 \cos\varphi_1 & -z_{2A}\cos\varphi_2 \\ -z_1 \sin\varphi_1 & -z_{2A}\sin\varphi_2 \end{bmatrix} \begin{Bmatrix} \ddot{\varphi}_1^2 \\ \ddot{\varphi}_2^2 \end{Bmatrix} := \mathbf{F}\ddot{\boldsymbol{\varphi}} + \mathbf{G}\dot{\boldsymbol{\varphi}}^2 \qquad (22)$$

By combining (10), (13), (21) and (22), after some algebraic manipulations, $\mathbf{F_S}$ is obtained:

$$\mathbf{F_S} = (\mathbf{M_S F} + \mathbf{I_{NS}})\,\mathbf{J_S^{-1}}\ddot{\mathbf{X}} + \left[\mathbf{M_S G} - (\mathbf{M_S F} + \mathbf{I_{NS}})\mathbf{W}\right]\left(J_{\mathbf{k}}^{-1}\dot{\mathbf{X}}\right)^{\mathbf{2}} \qquad (23)$$

4.4. Overall System Dynamics Model

In order to obtain the overall system dynamics equations of motion, expressed in a standard Cartesian form for robotic systems, we substitute (23) into (18):

$$\mathbf{S}\boldsymbol{\tau} = \left[r\mathbf{m} + \mathbf{SJ}\frac{\partial\boldsymbol{\beta}}{\partial\mathbf{X}} - r(\mathbf{M_S F} + \mathbf{I_{NS}})\mathbf{J_k^{-1}}\right]\ddot{\mathbf{X}} + \left[\mathbf{SC}\frac{\partial\boldsymbol{\beta}}{\partial\mathbf{X}} + \mathbf{SJ}\frac{\mathrm{d}}{\mathrm{d}t}\left(\frac{\partial\boldsymbol{\beta}}{\partial\mathbf{X}}\right)\right]\dot{\mathbf{X}}$$

$$-r\left[\mathbf{M_S G} - (\mathbf{M_S F} + \mathbf{I_{NS}})\mathbf{W}\right]\left(\mathbf{J_k^{-1}}\dot{\mathbf{X}}\right)^{\mathbf{2}} \qquad (24)$$

The expression above can be rewritten in standard matrix form:

$$\mathbf{S}(\mathbf{X})\boldsymbol{\tau} = \mathbf{M_{eqX}}(\mathbf{X})\ddot{\mathbf{X}} + \mathbf{N_X}\left(\mathbf{X},\dot{\mathbf{X}}\right) \qquad (25)$$

where:

$$\mathbf{M_{eqX}} = \left[r\mathbf{m} + \mathbf{SJ}\frac{\partial\boldsymbol{\beta}}{\partial\mathbf{X}} - r(\mathbf{M_S F} + \mathbf{I_{NS}})\mathbf{J_k^{-1}}\right]$$

$$\mathbf{N_X} = \left[\mathbf{SC}\frac{\partial\boldsymbol{\beta}}{\partial\mathbf{X}} + \mathbf{SJ}\frac{\mathrm{d}}{\mathrm{d}t}\left(\frac{\partial\boldsymbol{\beta}}{\partial\mathbf{X}}\right)\right]\dot{\mathbf{X}} - r\left[\mathbf{M_S G} - (\mathbf{M_S F} + \mathbf{I_{NS}})\mathbf{W}\right]\left(\mathbf{J_k^{-1}}\dot{\mathbf{X}}\right)^{\mathbf{2}}$$

and the dependence of the matrices on the Cartesian coordinates and velocities are made explicit.

5. Model Based Control Architecture

A control scheme suitable for CDDRs must not only ensure that the robot follows the desired reference trajectory but also guarantee that all cable tensions ti always keep positive values. In this work a control scheme based on the overall system Cartesian dynamics equations of motion is proposed to determine the Cartesian control force $\mathbf{S}(\mathbf{X})\boldsymbol{\tau}$ that the cables have to exert on the end-effector. Then, due to redundant actuation, a choice has to be made among the ∞^2 possible solutions to the motor torque vector τ that can exert the desired control force. A method is proposed, which is based on the solution of a linear programming problem, and which ensures all cable tensions are positive while minimizing the sum of all torques exerted by the motors.

5.1. Control Law

The following nonlinear-model-based control law is adopted:

$$\mathbf{S}(\mathbf{X})\boldsymbol{\tau} = \mathbf{M_{eqX}}(\mathbf{X})\left(\ddot{\mathbf{X}}_{\mathbf{ref}} + \mathbf{K_d}\dot{\mathbf{e}} + \mathbf{K_p}\mathbf{e}\right) + \mathbf{N_X}\left(\mathbf{X}, \dot{\mathbf{X}}\right) \tag{26}$$

where $\ddot{\mathbf{X}}_{\mathbf{ref}} \in \mathbb{R}^2$ is the second derivative of the desired reference trajectory $\mathbf{X_{ref}} = \left\{x_{ref}\ y_{ref}\right\}^T$, $\mathbf{e} \in \mathbb{R}^2$ is the tracking error between the desired and the actual trajectory $(\mathbf{e} = \mathbf{X_{ref}} - \mathbf{X})\dot{\mathbf{e}} \in \mathbb{R}^2$ is the tracking error rate, and $\mathbf{K_p} = \begin{bmatrix} K_{p_x} & 0 \\ 0 & K_{p_y} \end{bmatrix}$ and $\mathbf{K_d} = \begin{bmatrix} K_{d_x} & 0 \\ 0 & K_{d_y} \end{bmatrix}$ are the diagonal matrices of the proportional and derivative gains introduced in the control law to reduce the tracking error e. In the proposed control law, the control action $\mathbf{S}(\mathbf{X})\boldsymbol{\tau}$ is divided into two portions; a model-based portion:

$$\left[\mathbf{S}(\mathbf{X})\boldsymbol{\tau}\right]_{\mathrm{MB}} = \mathbf{M_{eqX}}(\dot{\mathbf{X}})\dot{\mathbf{X}}_{\mathbf{ref}} + \mathbf{N_X}\left(\mathbf{X}, \dot{\mathbf{X}}\right)$$

and a proportional-derivative servo portion:

$$\left[\mathbf{S}(\dot{\mathbf{X}})\boldsymbol{\tau}\right]_S = \mathbf{M_{eqX}}(\mathbf{X})\left(\mathbf{K_d}\dot{\mathbf{e}} + \mathbf{K_p}\mathbf{e}\right).$$

The chief advantage of such a scheme is that it allows linearizing of the system dynamics model, and in particular making the system appear as a unit mass. By combining (25) and (26) we get the following dynamic equation for the tracking error:

$$\ddot{\mathbf{e}} + \mathbf{K_d}\dot{\mathbf{e}} + \mathbf{K_p}\mathbf{e} = 0.$$

The design of the servo portion then is straight-forward: Gains are chosen to obtain some desired closed loop stiffness (by directly setting the elements of matrix $\mathbf{K_p}$) and specifying critical damping (i.e. $\mathbf{K_d} = 2\sqrt{\mathbf{K_p}}$). It is important to note that since the gain matrices $\mathbf{K_p}$ and $\mathbf{K_d}$ are chosen as diagonal, the servo control is accomplished independently for the x and y motions, even though the dynamics model is coupled.

5.2. Linear Programming Problem

The computation of the vector $\boldsymbol{\tau} \in \mathbb{R}^4$ of the cable torques producing the desired control force $\mathbf{S}(\mathbf{X})\boldsymbol{\tau}$ has the problem to invert the matrix $\mathbf{S}(\mathbf{X})$ which is non-square, but is underconstrained. As mentioned previously, among the ∞^2 possible solutions to this problem, it is necessary to choose a solution which always guarantees positive cable tensions. In this work a linear programming problem is solved to meet this requirement and to minimize the sum of the torques exerted by the motors. The problem is stated as follows:

$$\min_{\tau} \sum_{i=1}^{4} \tau_i \tag{27}$$

subject to the constraints:

$$\begin{cases} \sum_{i=1}^{4} -\tau_i \cos\theta_i = \mathfrak{J}_x \\ \sum_{i=1}^{4} -\tau_i \sin\theta_i = \mathfrak{J}_y \end{cases}$$

$$\mathbf{T} \geq 0 \Rightarrow \boldsymbol{\tau} \geq \mathbf{J}\ddot{\boldsymbol{\beta}} + \mathbf{C}\ddot{\boldsymbol{\beta}} \Rightarrow \begin{cases} \tau_i \geq J_1\ddot{\beta}_1 + c_1\dot{\beta}_1 \\ \vdots \\ \tau_4 \geq J_4\ddot{\beta}_4 + c_4\dot{\beta}_4 \end{cases} \tag{28}$$

where the symbols $\mathfrak{J}_x$ and $\mathfrak{J}_y$ have been adopted to denote the components along the x_0 axis and the y_0 axis of the Cartesian control force $\mathbf{S}(\mathbf{X})\tau$. The well-known simplex method for linear programming can be employed to solve such a problem.

Figure 5 shows a block diagram of the proposed control scheme. In order to simplify the task definition, trajectory planning is performed in the Cartesian space. However, since the Cartesian position $\mathbf{X}$ and its rate $\dot{\mathbf{X}}$ cannot be measured directly, it is necessary to calculate these values using the feedback for pulley angles $\boldsymbol{\beta}$ and velocities $\dot{\boldsymbol{\beta}}$ (output of the 'CDDR' block) as the inputs to the forward position ($\mathbf{X} = \mathbf{X}(\boldsymbol{\beta})$) and velocity ($\dot{\mathbf{X}} = \dot{\mathbf{X}}(\boldsymbol{\beta}, \dot{\boldsymbol{\beta}})$) kinematics problems. The analytical solutions to these problems have been presented in the sections above. Alternatively, if the measurement and calculation of Cartesian position via encoders on the pulley angles is not reliable, due to difficulties in measuring through the direct loading path and possible cable stretch and other uncertainties, the passive SCARA may be equipped with two encoders, from which the Cartesian position may be determined. The knowledge of the reference and actual Cartesian position, velocity and acceleration

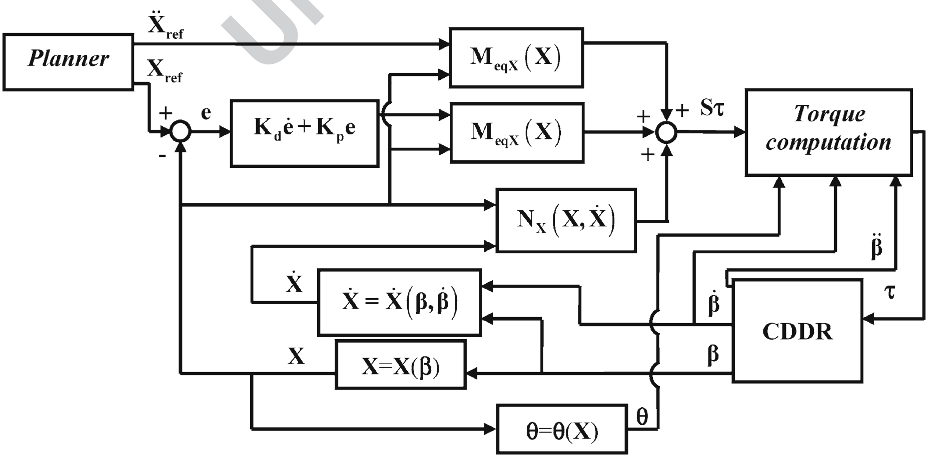

Figure 5 Proposed controller architecture.

Table I Simulation parameters

Parameter	Value	Units
L_A	0.7	m
L_B	1.1	m
z_1, z_2	0.49	m
w	$6.3 \cdot 10^{-2}$	m
h	$9 \cdot 10^{-2}$	m
s	$4 \cdot 10^{-4}$	m
M	4.2	kg
J_i $(i = 1, \ldots, 4)$	$8 \cdot 10^{-4}$	kg·m^2
c_i $(i = 1, \ldots, 4)$	0.01	N·m·s
r	$9 \cdot 10^{-3}$	m
m	20	kg

makes it possible to compute the model-based and the servo portions of the Cartesian control force $\mathbf{S}(\mathbf{X})\boldsymbol{\tau}$. Then, the solution of the above mentioned linear programming problem allows computing the actual torques to be exerted by the motors (output of the 'Torque computation' block).

6. Numerical Validation

The effectiveness of the proposed model-based control architecture is shown in this section by two simulation examples. The simulated tasks are for the CDDR

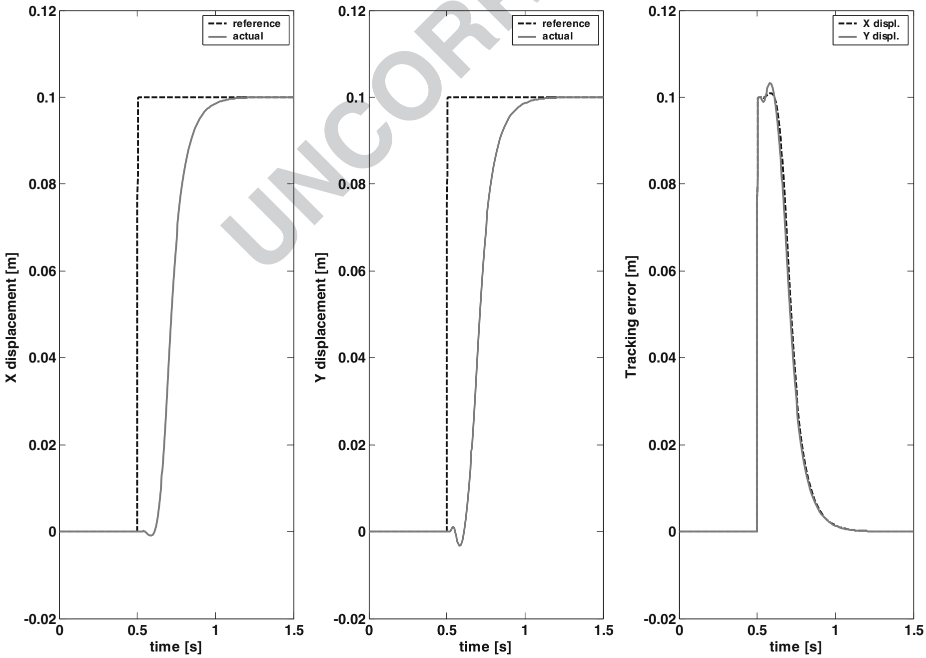

Figure 6 X and Y step responses and errors.

end-effector point X to trace a straight line and a circle in the plane. The results shown in this section have been obtained by assuming a CDDR payload m of 20 kg.

The geometric and inertial features of the CDDR are reported in Table I. In particular, the lengths L_A and L_B of the sides of the base polygon have been chosen as a rectangular workspace area comparable to the conventional industrial robot Adept SCARA 550 (top-view) workspace. The serial manipulator lengths z_1 and z_2 have been determined to allow the CDDR reach any point within the base polygon. Equal lengths have been chosen for the links. In order to prevent singular configurations, z_1 and z_2 have been taken slightly larger than the minimum theoretical value $0.5 * \sqrt{L_A^2 + (L_B/2)^2}$ (i.e. half the distance between the origin of reference frame {1} and the vertex A_3 or A_4). The links are assumed to be identical slender and hollow steel bars with rectangular cross-section. In Table I the link cross-section width is w, the height is h, the steel thickness is s, and the overall link mass is M. The link geometry has been determined so as to get a light structure ensuring limited and predictable off-the-plane deflections of the system with a payload up to 20 kg (3.6 times higher than the allowable SCARA 550 payload). Our proposed hybrid architecture CDDR has a high payload-to-weight ratio and a large workspace, which makes it an interesting prospective alternative to common industrial serial robots.

The servo portion of the controller has been tuned in simulation so as to get a satisfactory step response of the system. The gain matrix $\mathbf{K_p}$ has been chosen with

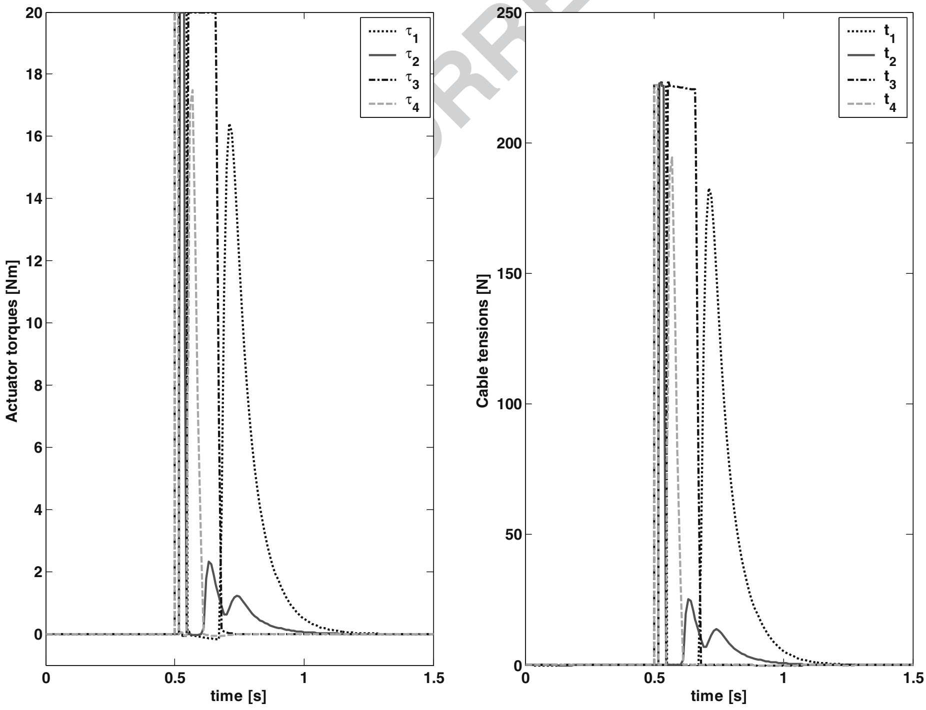

Figure 7 Simulated actuator torques and cable tensions.

equal gains of 289 on the diagonal. Consequently, critically damped response of the system is yielded by a diagonal matrix $\mathbf{K_d}$ with equal gains of $2\sqrt{289} = 34$ on the diagonal. As an example, Figure 6 shows the response of the system when identical step changes from 0 to 0.1 m are applied to the two components of the Cartesian reference $\mathbf{X_{ref}}$.

Figure 7 shows the computed actuator torques and cable tensions. Note that the actuator torques are assumed to be limited to 20 Nm. The atypical transient response of the system shown in Figure 6 immediately after the step changes are applied (slight negative motion), is a consequence of actuator saturation. No overshoot occurs and zero steady-state error is ensured. Figure 7 (right) shows the effectiveness of the method proposed to achieve positive cable tensions for all motion.

In Figures 8–10, the system capability in following a linear path is assessed. The path is a straight line from the origin of {0} to the point {0.3 m 0.3 m}, in 1 s. The initial and final Cartesian velocities and accelerations of the end-effector are prescribed to be zero. Quintic polynomials are adopted to satisfy the Cartesian position, velocity and acceleration constraints defined at the beginning and at the end of the path [6].

In Figure 8 the sequence of positions of the serial manipulator links during the simulated task are plotted to scale. For clarity, the cables are only shown in dashed lines at the starting and ending positions. Figure 9 shows that the proposed control scheme enables low tracking errors along both Cartesian axes, including a prompt return to zero error at the path end. Figure 10 shows the actuator torques and the

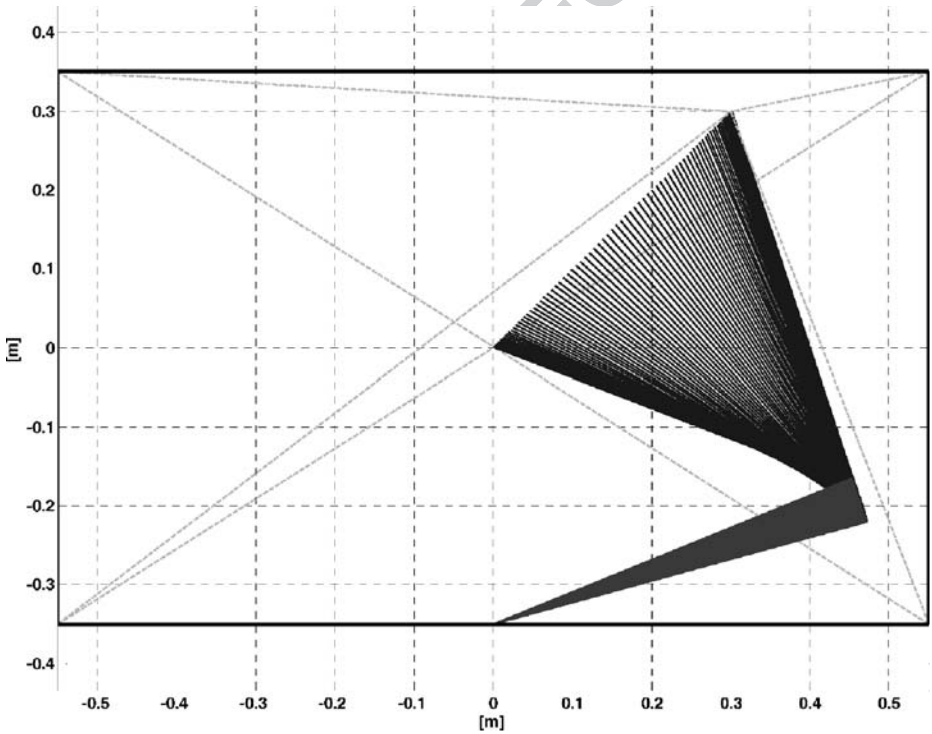

Figure 8 Straight-line motion dynamic simulation.

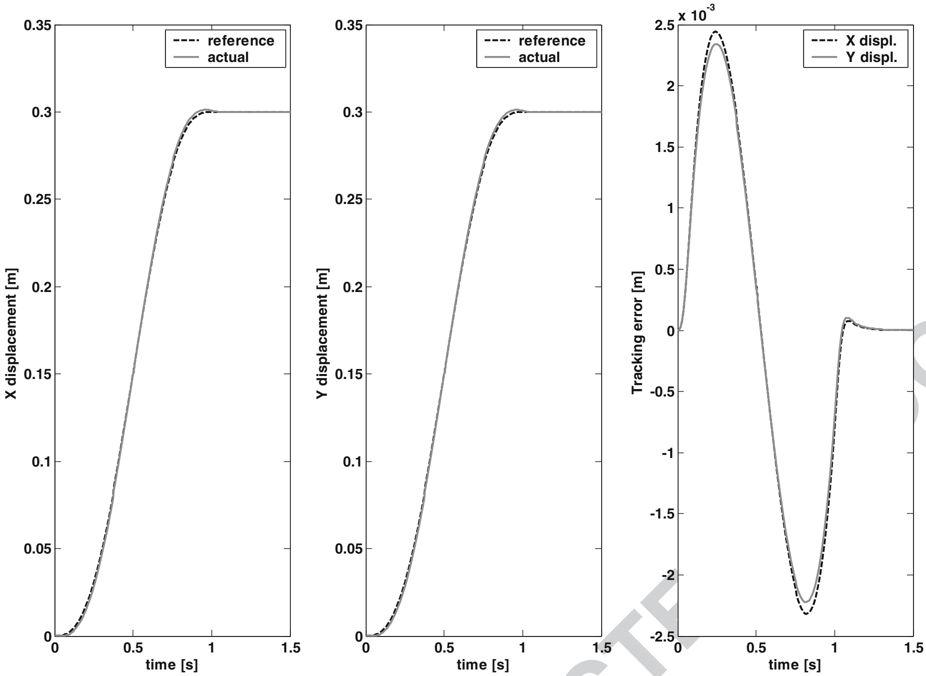

Figure 9 *X* and *Y* responses and errors for straight-line motion.

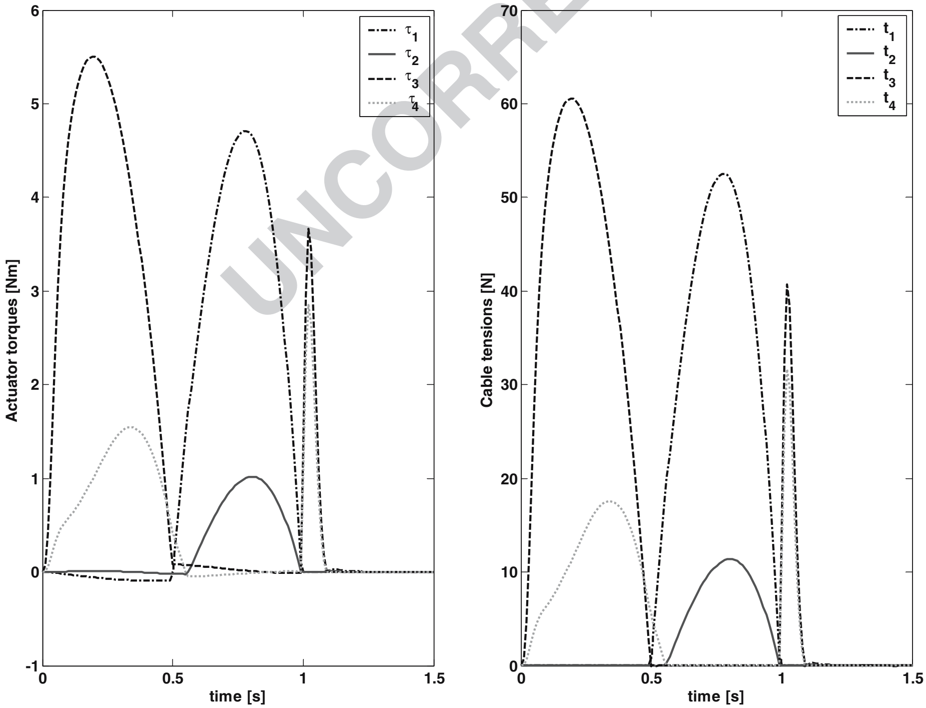

Figure 10 Straight-line motion actuator torques and cable tensions.

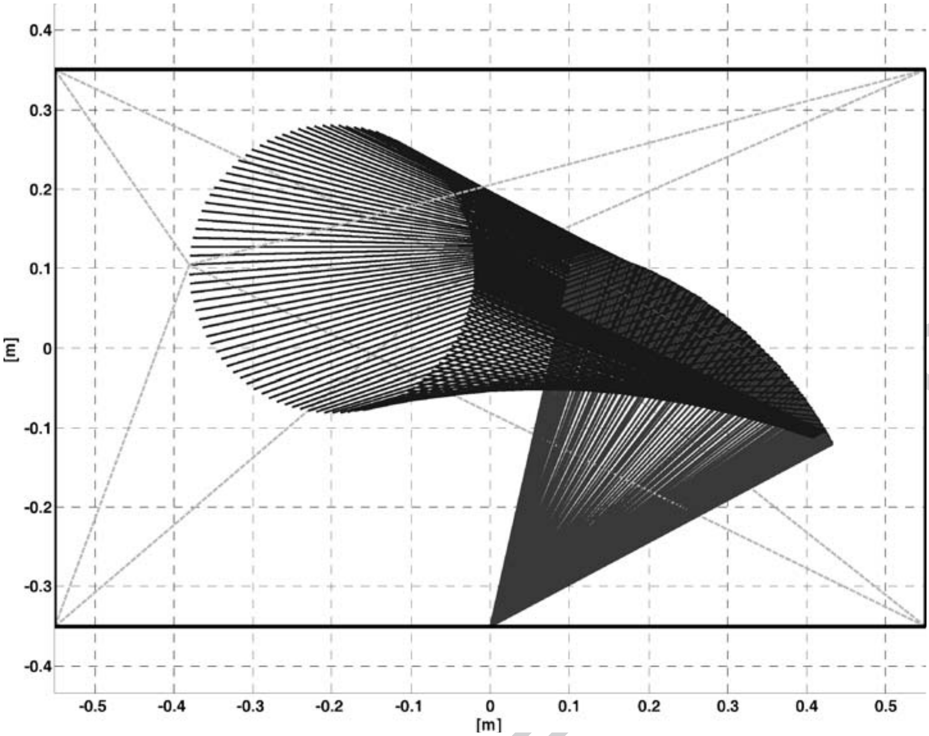

Figure 11 Circular motion dynamic simulation.

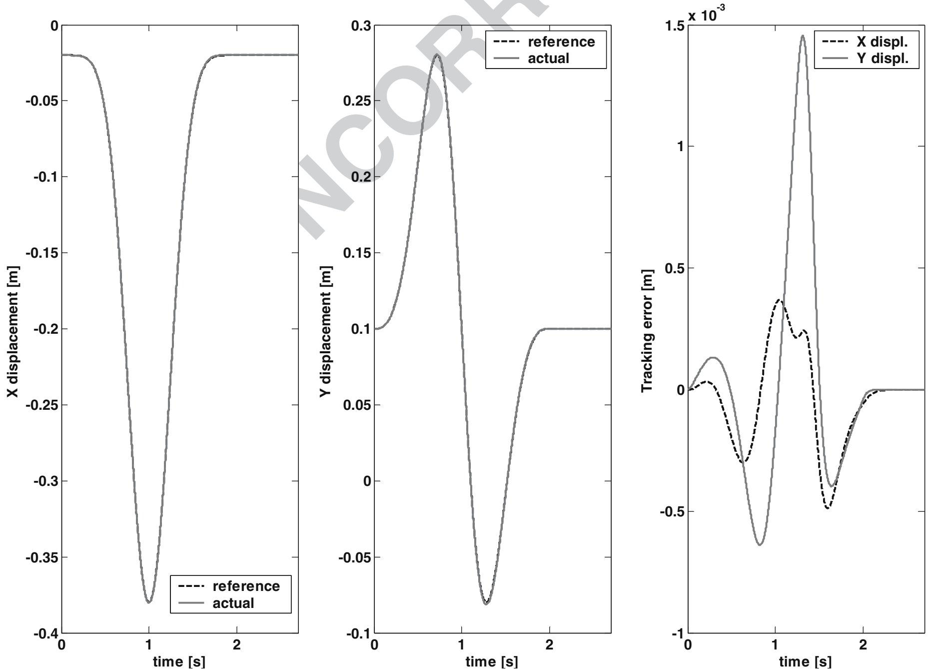

Figure 12 X and Y responses and errors for circular motion.

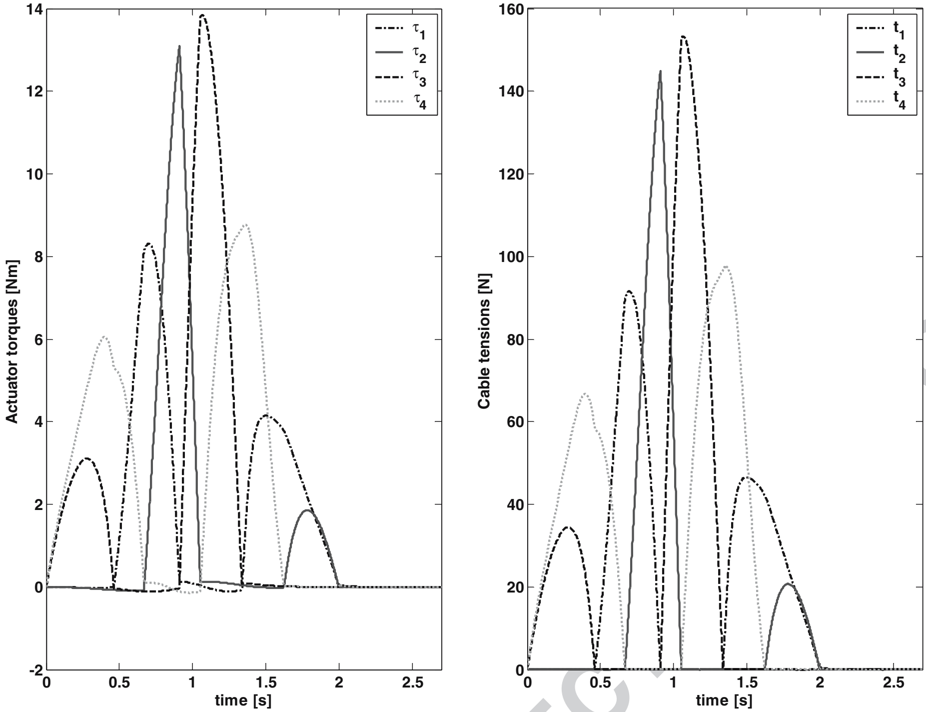

Figure 13 Circular motion actuator torques and cable tensions.

cable tensions for the prescribed dynamic motion. The former are always below the maximum value of 20 Nm; the latter are always positive, therefore meeting the fundamental requirement for CDDRs.

A final simulation test to assess the proposed control scheme performances is requiring the end-effector to trace a circular trajectory in 2 s. The circle is centered at point $\{-0.2 \text{ m } 0.1 \text{ m}\}$ with a radius of 0.18 m. Figure 11 shows the simulated task to scale. The cables are shown in dashed lines at the starting and midpoint of the path. In this test the polar angle is defined as the independent parameter for the circle. When the polar angle is equal to zero or 2π the end-effector is at point $\{-0.02 \quad 0.1 \text{ m}\}$, the starting and ending point of the path. The initial and final angular velocities and accelerations are set to zero. A quintic polynomial is employed to interpolate the initial and final polar angle values and to satisfy the angular velocities and accelerations constraints. The simulated results are summarized in Figures 12 and 13. Figure 12 shows that the tracking error is kept small, even when the velocity of the end-effector reaches the highest values (e.g. from time $t = 0.828$ to $t = 1.176$ s, the instantaneous tangential end-effector velocity magnitude is greater than 1 m/s). The error promptly goes to zero when the system reaches steady-state. Figure 13 again confirms that the proposed control scheme keeps the actuator torques below 20 Nm, while all the cable tensions are enforced to be positive. This is a consequence of the favorable payload-to-weight ratio of the designed CDDR, and implies that the actuators can exert the desired control force $\{\Im_x \, \Im_y\}^T$ on the end-effector. The low weight of the manipulator also allows low cable tensions, which simplifies the choice of cable material and cross-section (e.g. reinforced-nylon cables with a diameter of 3 mm would be adequate for the tasks considered in these simulations).

7. Conclusion

This article has presented a novel planar translational cable-direct-driven robot (CDDR). The primary novelty is inclusion of a passive planar two-degree-of-freedom SCARA-type serial robot to provide stiffness normal to the plane of motion. This allows the robot to be suspended rather than supported by the plane of motion. Also, the passive robot, if instrumented with two joint encoders at the passive R joints, can serve as an independent Cartesian metrology system. This could improve the required Cartesian feedback in the case of high masses and accelerations, when the encoder feedback from the active actuators may become unreliable due to measuring through the load path, cable stretch, and other uncertainties. Yet another potential benefit is that with the passive SCARA, there is structure at the end-effector which can provide moment resistance – this is not possible with many translation-only CDDRs that have been proposed.

The proposed robot has a high payload-to-weight ratio (despite the additional mass of the passive serial robot, which is much lighter than a comparable active serial robot) and resistance to forces normal to the plane of motion, due to gravity and environment interaction forces. Though this is a translational CDDR, end-effector rotations may be achieved by adding a robot wrist to the end of the passive serial arm (increasing the end-effector mass). Also, though the CDDR is planar, we can achieve 3D workspace by adding an active Z axis to the passive SCARA in the normal manner (also increasing the end-effector mass).

This paper has presented the novel CDDR with passive SCARA support, followed by the derivation of kinematics and dynamics equations and solutions, and a Cartesian controller architecture including a means of maintaining positive cable tensions for all dynamic motion while minimizing the total actuation torque. Simulation examples were presented for a double Cartesian step input, straight-line motion, and a circular trajectory. Simulation results show that the motions can be made subject to actuator torque limitations, with only positive cable tensions.

References

1. Aria, T., Osumi, H., Yamaguchi, H.: Assembly robot suspended by three wires with seven degrees of freedom, MS90-807, 11th International Conference on Assembly Automation. SME, Dearborn, Michigan (1990)
2. Albus, J.S., Bostelman, R., Dagalakis, N.G.: The NIST RoboCrane. J. Robot. Syst. **10**(5), 709–724 (1993)
3. Barette, G., Gosselin, C.M.: Kinematic analysis and design of planar parallel mechanisms actuated with cables. ASME Design Technical Conferences, Baltimore, MD (2000)
4. Campbell, P.D., Swaim, P.L., Thompson, C.J.: Charlotte robot technology for space and terrestrial applications, Article 951520, 25th International Conference on Environmental Systems. San Diego, SAE (1995)
5. Choe, W., Kino, H., Katsuta, K., Kawamura, S.: A design of parallel wire-driven robots for ultrahigh speed motion based on stiffness analysis. ASME Japan/USA Symp. Flexible Autom. **1**, 159–166 (1996)

6. Craig, J.J.: Introduction to Robotics: Mechanics and Control. Pearson Prentice Hall, Upper Saddle River, New Jersey (2005)
7. Mikulas, M.M. Jr., Yang, L.F.: Conceptual design of a multiple cable crane for planetary surface operations, NASA Technical Memorandum 104041, NASA LaRC. Hampton, Virginia (1991)
8. Oh, S.R., Agrawal, S.K.: Cable-suspended planar parallel robots with redundant cables: Controllers with positive cable tensions, IEEE International Conference on Robotics and Automation, pp. 3023–3028. Taipei (2003)
9. Roberts, R.G., Graham, T., Lippitt, T.: On the inverse kinematics, statics, and fault tolerance of cable-suspended robots. J. Robot. Syst. **15**(10), 581–597 (1998)
10. Shanmugasundram, A.P., Moon, F.C.: Development of a parallel link crane: Modeling and control of a system with unilateral cable constraints, DSC 57-1, ASME International Mechanical Engineering Congress and Exposition, pp. 55–65. San Francisco California (1995)
11. Shen, Y., Osumi, H., Arai, T.: Manipulability measures for multi-wire driven parallel mechanisms. IEEE International Conference on Industrial Technology, pp. 550–554 (1994)
12. Shiang, W.J., Cannon, D., Gorman, J.: Dynamic analysis of the cable array robotic crane. IEEE Int. Conf. Robot. Autom. **4**, 2495–2500 (1999) (Detroit Michigan)
13. Williams, R.L. II, Gallina, P.: Translational planar cable-direct-driven robots. J. Int. Robot. Syst. **37**, 69–96 (2003)
14. Yamamoto, M., Yanai, N., Mohri, A.: Inverse dynamics and control of crane-type manipulator. IEEE/RSJ Int. Conf. Intel. Robot. Syst. **2**, 1228–1233 (1999) (Kyongju, Korea)

AUTHOR QUERY

NO QUERY